Peer-reviewed version available at *Atmosphere* **2017**, *8*, , 95; doi:10.3390/atmos8060095

Article

Intercomparison of MODIS and VIIRS Fire Products in Khanty-Mansiysk Russia: Implication for Characterizing Gas Flaring from Space

Ambrish Sharma [1] and Jun Wang [1,2,*]

1 Department of Earth & Atmospheric Sciences, University of Nebraska, Lincoln, NE 68588, USA; ambrish.sharma@huskers.unl.edu
2 Center for Global and Regional Environmental Research, the University of Iowa, Iowa City, IA 52242, USA
* Correspondence: jun-wang-1@uiowa.edu; Tel.: +1-319-353-4483

Abstract: Gas flaring is commonly used by industrial plants for processing oil and natural gases in the atmosphere, and hence is an important anthropogenic source for various pollutants including CO_2, CO, and aerosols. This study evaluates the feasibility of using satellite data to characterize gas flaring form space by focusing on the Khanty Mansiysk Autonomous Okrug in Russia, a region that is well known for its dominatingly gas flaring activities. Multiple satellite-based thermal anomaly data products *at night* are inter-compared and analyzed, including MODIS (Moderate Resolution Imaging Spectroradiometer) Terra level-2 Thermal Anomalies product (MOD14), MODIS Aqua level-2 Thermal Anomalies product (MYD14), VIIRS (Visible Infrared Imaging Radiometer Suite) Active Fires Applications Related Product (VAFP), and VIIRS level-2 data based Nightfire product (VNF). The analysis compares and contrasts the efficacy of these sensor products in detecting small, hot sources like flares on the ground in extremely cold environments such as Russia. We found that the VNF algorithm recently launched by NOAA has the unprecedented accuracy and efficiency in characterizing gas flares in the region owing primarily to the use of Shortwave Infrared (SWIR) bands. Reconciliation of VNF's differences and similarities with other nighttime fire products is also conducted, indicating that MOD14/MYD14 and VAFP data are only effective in detecting those gas flaring pixels that are among the hottest in the region. Validation of VNF product of gas flaring location with Google Earth images are made. It is shown that that VNF's estimates of gas flaring area (the area of gas flaming) agree well the counterparts from Google images with a linear correlation of 0.91, highlighting its potential use for routinely monitoring emissions of gas flaring from space.

Keywords: nighttime fires; gas flaring; MODIS; VIIRS; Khanty-Mansiysk Russia

1. Introduction

Gas flaring is a global environmental hazard severely impacting air quality, economy, climate, vegetation and public health (Ismail & Umokoro, 2012). According to World Bank estimates (Elvidge et al., 2009), over 150 bcm (billion cubic meters) of natural gas is being flared or vented globally each year, which adds about 400 million tons of carbon dioxide to the atmosphere in addition to other harmful impacts. Flaring is a high-temperature oxidation process to burn combustible components, which mostly constitutes hydrocarbons of waste gases from industrial operations (Gervet, 2007). It is widely used to dispose-off economically unprofitable waste gases emerging with oil but it also acts as a safety device providing protection from over pressuring of vessels. Profuse amount of world's energy supply are continuously lost through the flaring of gas, contributing to the global carbon emission budget (Casadio et al., 2011). Apart from greenhouse gases like methane and carbon dioxide and pollutants like, NO_2, SO_2 and CO, the flares contain widely-recognised toxins, such as benzene, benzopyrene, carbon disulphide (CS_2), carbonyl sulphide (COS) along with harmful metals such as

mercury, arsenic and chromium. These emissions pose a great threat to human health, built up environment and social well-being of inhabitants of host community (Nwanya, 2011). Therefore, it is essential to characterize gas flaring activity and its associated emissions, both spatially and temporally.

The objective of this paper is to evaluate the feasibility of using data from multiple satellite sensors to monitor gas flaring from space. In contrast to the ground-based observations, satellite remote sensing provides significant spatial (and sometimes temporal) advantages because of the routine and global coverage by the satellite sensors. The earliest detections of gas flaring using satellite remote sensing data date back to the early 1970s, when Croft, 1973 observed night-time imagery (mainly over Africa) from a lowlight sensor (operating in spectral range of 0.4-1.1 μm) belonging to the United States Airforce DAPP (Data Acquisition and Processing Progam) system, and found gas flares to be the brightest features observed in visible band. He used the imagery from sensor (DAPP system now called DMSP, Defense Meteorological Satellite Program) again in 1978 (Croft, 1978) along with Landsat Multi-spectral Scanner System to observe gas flares in many parts of the world including Algeria, Libya, Nigeria, Persian Gulf, Siberia and Mexico. He used visual identification and manual analysis procedures for the identification of flares from the images and reasserted that the gas flares associated with world's major oil fields were the brightest man-made features observed from space. Further, Muirhead and Cracknell (1984) used the daytime imagery from NOAA's AVHRR (Advanced very high resolution radiometer) to detect off-shore gas flaring sites in the North Sea. Their detections were based on the brightness values observed during daytime in the infrared channel (3.55 μm - 3.93 μm) of AVHRR, from the pixels containing gas flares. Much later the DMSP's Operational Linescan system products were used to produce maps of gasflares, fishing boats, fires and human settlements for 200 nations (Elvidge et al., 2001) as a part of first study to detect gas flaring globally. Further analyses of DMSP-OLS products provided the first record of long term (1994-2005) gas-flaring volumes (Elvidge et al., 2007) through ad-hoc calibration method and later these flaring and emission estimate products were extended to 2008 (Elvidge et al., 2009). Although these studies were able to characterize some gas flaring sites but their procedure relied on visual inspection of images (circularity and bright centres of flares), which was not time efficient. Also the spatial resolution of the instruments (e.g., smoothed nominal spatial resolution of 2.7 km for DMSP-OLS) wasn't usually high enough to resolve accurately for flare location, particularly if the flares are situated in proximity of bright urban areas.

The first study to objectively identify hot sources such as flares was done by Matson and Dozier (1981) who were able to identify some gas flares from oil fields by using hot source signal in MidWave InfraRed, MWIR (~3.7 μm) and LongWave InfraRed, LWIR (~11 μm) spectrums from the nighttime AVHRR (onboard NOAA-6) imagery. The capability of these bands highlighted by them for fire monitoring formed the basis of many fire detection algorithms (MODIS, VIIRS, AVHRR etc.) developed afterwards (Weaver et al., 2004; Giglio et al., 2003; Csiszar et al., 2014). A limitation of the fire algorithms based on MWIR and LWIR bands is that the measured brightness temperature is dependent on the background temperature which means the total radiance observed by the satellite instrument is the result of both burning (subpixel fire) and non-burning fractions (background) of the ground pixel. This becomes a shortcoming for hot spot detection in cold areas such as Canada and Russia (Casadio et. al, 2011). Later, an active flare detection algorithm for global flare monitoring was developed by Casadio et al. (2011) using ATSR (Along Track Scanning Radiometeres) SWIR band imagery. The use of shortwave infrared (SWIR) band overcomes the problem faced by standard fire product algorithm, for the extremely hot sources like gas flares. Since the background contribution to SWIR during night-time is negligible in it, the signal to noise ratio is high. They further revised their algorithm by an integrated use of ATSR and SAR (Synthetic Aperture Radar) night-time products for North Sea flare detections (Casadio et al., 2012). This method offered significant improvement over previous manual detection methods, but the low spatial resolution of ATSR instrument (1000 m) still posed a challenge towards the accuracy of flare detection.

More recently, Elvidge et al. (2013) have developed an algorithm using SWIR bands (1.6 μm channel as primary detection band) data from high resolution VIIRS nightime imagery for global fire

activity monitoring during nightime. The product also uses 5 more spectral bands in the near infrared, short wave infrared, medium wave infrared region and a panchromatic Day-Night band (DNB) for additional quality check on detections, but the product doesn't discriminate active flares from other fire sources such as biomass burning and forest fires. Anejionu et. al. (2014) also developed an objective flare detection method based on multispectral infrared band data from Landsat imagery (having high spatial resolution); but the detections were confined to Niger data only and their method was handicapped by limitations such as low frequency of available cloud free images and unavailability of night-time Landsat data. Nevertheless, all these efforts have paved way for more precise and automated detections of gas flares globally, and so moving forward, a comprehensive study of these new active gas flaring products is essentially required.

Despite the availability of high resolution data from new generation satellite sensors, there have been only a limited number of studies specifically targeted to monitor gas flaring from space, and satellite-based fire or hot-spot products are not well-validated for cases of gas flares. Therefore, a detailed analysis of performance of night-time fire products over gas flaring regions is necessary. The objective of this study is to assess the performance of the existing fire products and to reconcile for the differences in the detections by MODIS and VIIRS products with the newly developed VNF product over the test region. The study aims to explain the underlying differences between nocturnal fire detections from MOD14, MYD14, VAFP and VNF products. It is well known that factors (listed in Table 1) such as differences in sensor characteristics, spatial resolution and along-scan aggregation schemes play an important role in resultant fire detections differences (even when sensors have similar orbital characteristics, as in the case of VIIRS and Aqua). In extension to these factors, the study investigates how the choice of primary detection spectral bands affects the fire detections, and looks into the validation of parameters reported by the VNF version 1.0 product.

Table 1. Differences in Algorithms of fire products.

	MODIS Fire Product	VIIRS Active Fire	NOAA VNF
Primary Detection Band	4µm , 11µm channels	4µm , 11µm channels	1.6µm channel
Treatment of Clouds	Cloudy Pixels Pre-screened	Cloudy Pixels Pre-screened	Completely or Partially Cloudy Pixel considered
Solar Contamination	Observations ≥ 85^0 SZA	Observations ≥ 85^0 SZA	Observations > 95^0 SZA
Auxiliary Info	Fire Radiative Power, Geolocation, Geometry	Geolocation, Geometry	Sub-pixel fire area , temperature and radiant heat, Geolcation, Geometry
Spatial Resolution	Ikm at Nadir	750 m at Nadir	Variable
Aggregation	None	Sub-pixel aggregation across scan	N/A
Potential Pixel Selection	$T_4 > 305$ and $\Delta T > 10$	$T_4 > 305$ and $\Delta T > 10$	Radiance values above calculated threshold

The test region used for the study is Khanty Mansiysk Autonomous Okrug- Russia. The choice of the region is based on the fact that Russia has emerged as the biggest flaring region of the world lately (Elvidge et al., 2007). Russia is believed to be responsible for a quarter to a third of global associated gas flaring. Data from NOAA shows Russia flares about 35 bcm of gas per year and the related economic losses account for $5 billion per year (worldbank.org). The satellite-based estimate of gas flaring volumes reported from Khanty Mansiysk alone account for more than 50% of total Russian flaring (Elvidge et al., 2007). Moreover the official and unofficial data on associated gas resources and utilization volumes isn't accurate and doesn't reflect actual extent of flaring. The

discrepancies are because of lack of adequate instrumentation and equipment to generate precise statistics on flaring volumes. According to the Govt. Of Khanty Mansiysk Autonomous District, only the half of flare units operating in it were equipped with metering devices as of 2007 which worsens the problems for accurate estimation of flaring volumes (Knizhnikov and Poussenkova, 2009).

The large amount of gas flaring in Russia has a significant impact on climate. Russian gas flares annually produce almost 100 million tons of CO_2 emissions, given the entire gas is flared efficiently. However, due to large inefficiency in burning, the much more harmful greenhouse gas is emitted as well. The volume of soot emissions caused by the associated gas flaring is approximately 0.5 million tons/year. Moreover, the presence of gas flares in such large amount is hugely detrimental to public health too. Sizeable concentrations of nitrogen oxides and sulphur oxides, along with carbon monoxide etc. are recorded near the vicinity of the flare (Knizhnikov and Poussenkova, 2009), contributing to the increased cases of lung and bronchi cancer, damages of nervous system, liver and eyesight in the gas flaring affected communities. Therefore it is highly important to study the large gas flaring regions in Russia such as Khanty Mansisyk and satellite remote sensing offers significant benefits in that aspect.

2. Experiments

2.1. MODIS Thermal Anomalies and Fire Products (MOD14 and MYD14)

The MOD14 and MYD14 level 2 Thermal Anomalies and Fire Products are derived from the radiances observed in the MWIR and LWIR channels of MODIS instruments residing on NASA EOS-Terra and EOS- Aqua satellites respectively. Both MODIS Aqua and MODIS Terra acquire data twice a day (once each in nighttime and daytime) about 3 hours apart from each other, and are used to produce level-2 swath data at 1 km resolution on daily basis. The detection algorithm is based on the brightness temperature derived from MODIS 4 μm and 11 μm channels (Justice et. al, 2002). The detection function on either the absolute test, where the derived brightness temperature of the potential fire pixel is more than the predetermined threshold, qualifying it as a fire containing pixel or the contextual tests where a series of tests are employed to detect fire pixels having a temperature difference with the background large enough so as to be qualified as a fire pixel. Apart from providing the geolocation of the fire detected, the science data sets in the product provide information on fire mask, fire radiative power and quality flags on algorithm. Both of the products have attained Validation Stage 3 (uncertainties in the product are well quantified from comparison with reference in situ or other suitable reference data) for which active fire reference data from ASTER and LANDSAT- TM have been used (Morisette et al., 2005; Csiszar, Morisette and Giglio, 2006; Scrhoeder et al., 2008).

2.2. MODIS Thermal Anomalies and Fire Products (MOD14 and MYD14)

The VIIRS AFARP (Active Fire Applications Related Product), called VAFP in the study, is the fire detection product derived from radiances obtained in MWIR and LWIR channels of VIIRS instrument aboard SUOMI-NPP. The EOS MODIS Collection 4 Fire and Thermal Anomalies Algorithm forms the basis of the algorithm for this product (Csizar et. al, 2014). The tests used to identify fire containing pixels in VAFP are similar to the ones used in the MODIS fire detection algorithm. The primary channels used for algorithms are M13 (3.9 - 4.1 μm) and M15 (10.2 -11.2 μm) bands. Although the spectral placement of these channels is a little different from MODIS, the basic algorithm is applicable to these channels. VIIRS has a similar overpass time as MODIS Aqua but they differ in spatial resolution (VIIRS having higher spatial resolution than MODIS) and along scanline aggregation schemes (Polivka et al., 2015); these differences can result in the difference in fire detection between MODIS and VAFP products. The VAFP was released to the public with a provisional level maturity on 16 Oct 2012. The provisional quality is described as: product may not have optimal quality; version control is still in effect; general research community is encouraged to participate; incremental product improvements are still occurring and it's ready for operational evaluation.

2.3. MODIS Thermal Anomalies and Fire Products (MOD14 and MYD14)

The Nightfire product, VNF developed by Elvidge et al. (2013), provides nocturnal fire monitoring data globally for each day. The product operates on level-2 SDR (Sensor Data Records) data from VIIRS sensor aboard Suomi - NPP. It uses radiances observed in visible, Near Infrared (NIR), SWIR, MWIR and DNB (Day Night Band) spectra, but is primarily based on detections in SWIR band (1.6 μm) that corresponds to M10 band in VIIRS. As mentioned earlier, the SWIR bands prove advantageous for hot source detection during nighttime as high radiant emissions from the hot sources recorded by them stands out in contrast to the sensor noise recorded otherwise. The product provides crucial parameters such as subpixel fire area, radiant heat, radiant heat intensity and fire temperature based on Planck curve fitting, along with the geolocation and other metadata such as radiance thresholds, quality flags, and cloud mask etc.

Figure 1. Projected map of test region (in red boundaries) enclosing Khanty Mansiysk- Autonomous Okrug, Russia.

2.4. Study Region and Time Period

The Khanty Mansisyk region has a sub-arctic climate which means the winters are very long and cold and the summers are short and cool to mild in terms of temperature. The warm season lasts here from late May to early September and the cold season lasts from late November to early March. The precipitation is fairly low (~ .21 inches/year) and is heavier in winter than in summer. Over the entire year the most common forms of precipitation are light rain, light snow and moderate snow. The cloud cover is more than 80% throughout the year (weatherspark.com). The clearer part of the year begins around mid-April and the cloudier part of the year begins around late August and sustains through mid-April. Therefore the summer months, April- August (having less cloud cover) are used for analysis in this study.

We used MOD14, MYD14, VAFP and VNF products over a 10° x 10° region (55° N - 65° N, 65° W -75° W) that encloses our study area Khanty Mansiysk Autonomous Okrug in Russia and also some neighboring states like Komi, Yamalia and Tyumen Oblast. Night-time data from all the products was acquired for five summer months of 2013. Fig. 1 shows the map of study region and Fig. 2 shows detections by the four different fire products during the period May - July 2013. It is notable that the number of hotspots detected during nighttime by the VNF product is much higher than the counterparts by MODIS and VIIRS official fire products. Most of the VNF detections are in

fact the abundant gas flares found in the region of Khanty-Mansiysk, Russia. These gas flares are not picked up by the MODIS and VIIRS fire products because they are primarily designed to detect wild fires that usually have bigger surface area and burn at lower temperatures rather than small bright hot sources like gas flares. VNF on the other hand consciously utilizes the shortwave bands to detect hot sources like flares even with small surface areas of the order few m^2 only. Since the gas flares are quite abundant in the region and the VNF product is able to detect them while other products fail to do so, the cumulative impact on the number of detections is much larger when we observe detections on a larger space for a couple of months. Nevertheless, we will analyze the reasons for the differences of these products in detail in section.

3. Analysis of algorithm differences

As illustrated by Fig. 2. there are conspicuous large differences between the detections done by the VNF product and the MODIS & VIIRS active fire products. Since the VNF product detects the most flaring activity because of the use of shortwave bands, it was used to demarcate the gas flaring regions. The flaring regions were demarcated in order to quantify the number of detections by the different fire products within and outside of these regions to evaluate their performance. The entire study area was broken down into a collection of 0.25° × 0.25° grids. Persistence of detection within the grids and associated high temperature were used as the criteria for delineate the gas flaring regions. The hotspots detected by the VNF were collocated over the reference grid for each day (a total of 153 days were used). Only the detections having cloud mask as clear and having temperatures higher than 1600 K (temperature criterion from Elvidge et. al, 2013) were used and marked as valid, rest detections were filtered. Total number of valid detections within each grid was recorded for each day. For each grid, a frequency counter was also set to count the number of days when clear-sky, hot spot activity was observed in it. If one or more valid detections were found in a grid on a given day, a count was added to counter of the grid. At the end the grids having at least 15 days (almost 10% of total days studied) of hotspot activity within them were highlighted as most probable areas having flaring activity in them.

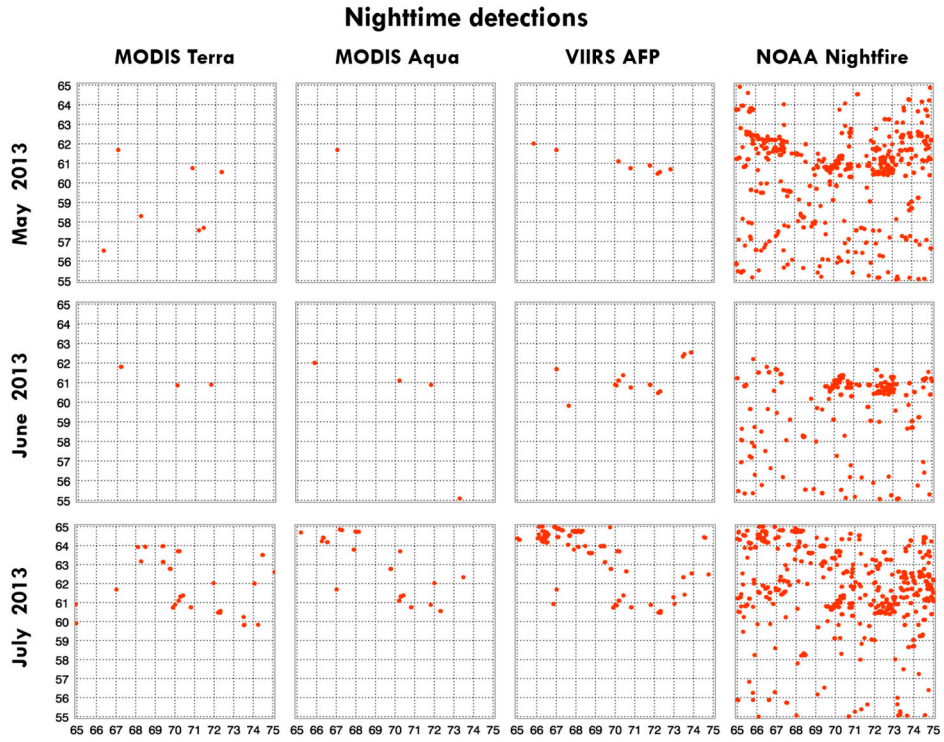

Figure 2. Night-time fire detections by different products over the study area during summer 2013. The considerable difference in detections between VNF and other products is due to more detections of flare in the region by the VNF.

Preprints (www.preprints.org) | NOT PEER-REVIEWED | Posted: 8 May 2017 doi:10.20944/preprints201705.0051.v1

Peer-reviewed version available at Atmosphere 2017, 8, , 95; doi:10.3390/atmos8060095

Following the procedure above, a total of 99 such grids were found (75 of those grids showed hotspot activity in them for at least 30 days). Figure 3 shows these areas (as yellow boxes) along with detections from MODIS Terra, MODIS Aqua and VIIRS active fire products during the night time for five summer months of 2013.

Figure 3 describes how the detections from various fire products are aligned with the probable flaring areas. A quantitative analysis for these detections is tabulated in Table 2, displaying total number of detections by these sensors on a monthly basis within and outside gas flaring regions. As expected and observed earlier in Fig. 2, VNF showed maximum number of hotspot counts over the entire region, much more than other night-time product studied. VAFP (following VNF by a huge margin) was found to have more number of detections (about 5 times) than MODIS Terra and Aqua. In terms of alignment with the gas flaring areas, ~ 47% of nighttime detections from MODIS Terra were found within the gas flaring zones (grids showing persistent, high temperature fire activity), whereas ~ 67% and ~55% of nighttime detections by MODIS Aqua and VAFP respectively were found in the gas flaring zones.

Detection counts recorded in each grid from the VNF product were divided into two categories based on associated brightness temperatures, a) T_B (0< T_B <1600K) and b) T_B (T_B ≥1600K), to see how detections from both these temperature ranges align with the gas flaring regions, with the latter range representing hotter sources (temperature characteristic of flares). It also helps in characterization of the hot source type (gas flares or forest fires, biomass burning etc.) found in the study area along with spatial pattern of their occurrence. ~77% of the total number of valid detections by the VNF product over the entire study region belonged to category (b) (T_B ≥1600 K) which indicates the dominance of the flaring activity in the area. About 52% of the detections belonging to category (a) were found in the gas flaring zones and ~ 95% of the detections from category (b) were found in the flaring zones.

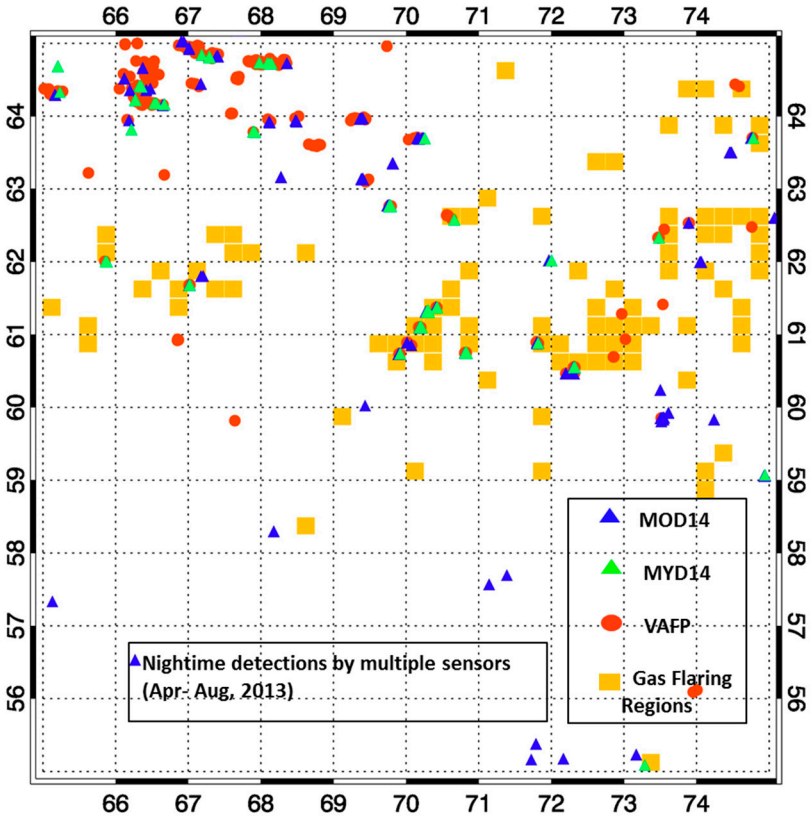

Figure 3. Nocturnal detections by different sensors over the gas flaring regions in the study area (April-August 2013).

Table 2. Multi-sensor fire detection during summer 2013 over the study area.

Date Nightitimt	MOD14 (MODIS Terra)			MYD14 (MODIS Aqua)			VAFP (VIIRS)			(VIIRS) 0< T_B≥ 1600			T_B		VNF <1600K	
	Total	In**	Out*	Total	In	Out	Total	In	Out	Total	In	Out	Total	In	Out	
April '13	07	02	05	02	02	00	17	15	02	551	301	250	2603	2461	142	
May '13	11	07	04	01	01	00	45	45	00	339	161	178	1476	1400	76	
June '13	04	02	02	05	04	01	52	36	16	86	85	01	370	357	13	
July '13	56	23	33	49	26	23	314	137	177	983	569	414	3004	2897	107	
August '13	59	30	29	27	23	04	138	81	57	1359	852	507	4952	4706	246	

* In or out gas glaring regions shown in Fig. 3

Since the fire activity estimated by the VNF product was astoundingly much more than other official fire products like VAFP and MOD14, MYD14 etc., we decided to look deeper into the VNF product to comprehend it functioning better, and also to see how the differences could be better appreciated and reconciled. The next section therefore deals with NOAA VNF algorithm, its comprehension and replication and an approach to understand the underlying basis of the vast differences in the monitored fire activity.

4. Reconciliation between VIIRS and VNF

4.1. Reconciliation with replication and sensitivity analysis of VNF algorithm

To understand the functioning of the VNF algorithm, we replicated the algorithm in the same fashion as described in the work by Elvidge et al. (2013). The replication was confined only to the hotspot detection and threshold calculation part; we did not delve into the hot source area and temperature estimation part as performed by the authors using Planck curve fitting. The primary reason to perform the replication is just to familiarize oneself more with the intricate details and working of a product which was much more efficient in detecting flares than others, but the process eventually revealed some discrepancies found in the version1.0 of the product. Detections in 5 VIIRS bands –M10, M7, M8, M12 and M13 were performed using VIIRS level 2 data and compared to VNF. A small sub region of the study area showing hot spots persistently was chosen and level 2 data was collected for a random day (05 May 2013). Figure 4 shows that we are able to replicate the results of VNF. After replicating VNF product with multispectral data and gaining insight into the way it worked, we probed further into how such vast differences in nighttime fire detection (mainly flares in this particular case) between this product and other official fire products could be reconciled.

VIIRS nocturnal fire detection is primarily based on MWIR bands (Giglio et al., 2003), following the suit from MODIS fire products (Csiszar et al., 2014). The choice of primary spectral band by these products is one of the most important factors responsible for the remarkable difference in detections between VNF and other fire products eventually. The peak radiation

Preprints (www.preprints.org) | NOT PEER-REVIEWED | Posted: 8 May 2017 doi:10.20944/preprints201705.0051.v1

Peer-reviewed version available at Atmosphere 2017, 8, , 95; doi:10.3390/atmos8060095

emitted from the typical fire surface (temperature ~1000 $\pm$ **200** K) lies mostly near the mid wave infrared region of the electromagnetic spectrum, but the gas flares burn at very high temperatures (~1500 $\pm$ **200** K) and thus their peak radiant emissions are at much shorter wavelengths (i.e. in short wave IR). Therefore spectral bands operating in SWIR such as VIIRS M10 (~1.6 μm) used as a primary detection band by the VNF product provide an efficient in detecting both inland and offshore gas flaring sites globally. Another advantage that SWIR bands provide is that the background contribution to night-time radiance in them is quite low compared to the detector noise that is recorded by them (Casadio & Arino, 2008). Hence pixels containing hot sources stand out in these bands with their high radiance values and low contribution from background noise. Apart from choice of primary spectral band, a significant factor for different detections is the treatment for clouds by these products. While MODIS and VIIRS discard the pixels contaminated by clouds even partially, the VNF product doesn't discard the pixels with cloud cover. The developers of the VNF product while studying gas flares found that gas flares were being consistently misidentified as having cloud cover because of a spectral confusion and pixels were being marked as partially or completely cloudy (Elvidge et. al, 2013). They used a cloud clearing algorithm to reset the cloud mask values for gas flares associated with hot pixels identified by them as potential flares.

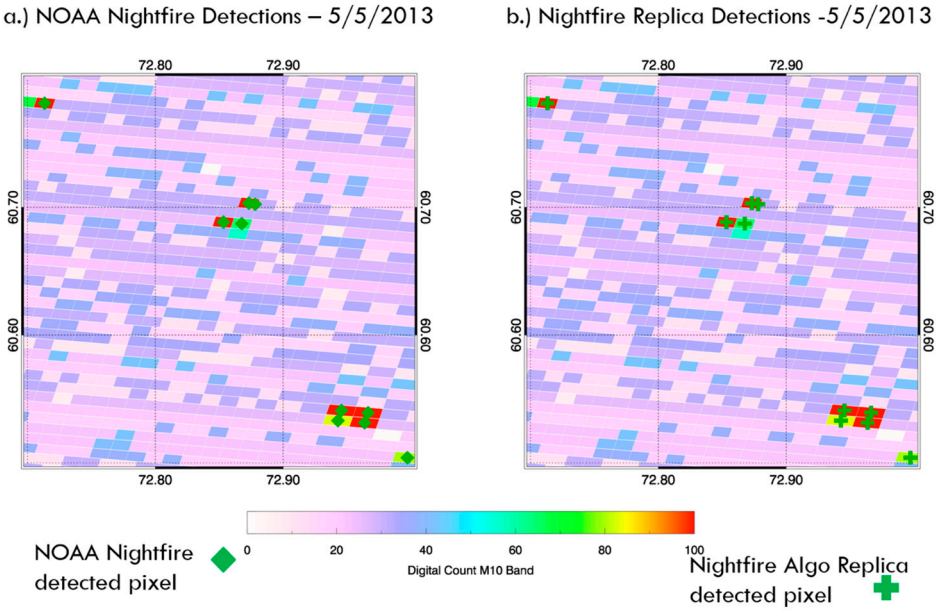

Figure 4. NOAA VNF and VNF Replica: Nighttime M10 band detections.

Other than these known factors we performed some case studies using days where both Nightfire and VAFP detected some fire activity in the study region, to see if the VNF detections could be made to match VAFP detections as an aid to determine crucial factors that lead to sizeable differences. We used the VNF replica that we developed to meet our purpose.

Case 1: July 04th, 2013; Area (latitude: 60°-61.5°, longitude: 70.5°-72°). Only two counts of fires were reported by the VAFP in the small target region, but the M10 VNF replica gave out 13 counts of hotspots in the same region (Fig. 5c, 5d). We increased the threshold 5 times the calculated value (in Digital Counts) for the M10 band in VNF Replica, and the number of hotspots detected with this new higher threshold were reduced to 7. These 7 hotspots still contained the 2 hotspots seen by VAFP. Upon stepping up the threshold further (10 times now the original M10 threshold in DC), only 4 detections from the VNF replica were observed, again identifying 2 hotspots seen by VAFP (Fig. 5e, 5f). When the threshold was raised 30 times, the exact spots were matched by the two products. It was concluded from this particular case study that the detections from the two products could be matched by increasing the threshold manifolds and VAFP is also detecting hotspots that have really high DN values in the M10 band. One of the hotspots detected by VAFP and VNF replica shows industrial settlement vaguely when looked into with zoomed in Google

Preprints (www.preprints.org) | NOT PEER-REVIEWED | Posted: 8 May 2017 doi:10.20944/preprints201705.0051.v1

Peer-reviewed version available at Atmosphere 2017, 8, , 95; doi:10.3390/atmos8060095

imagery (Fig. 5b) and there is a good probability of it being flow station for gas flares. Further zoom was unavailable to confirm it and the other spot could not be verified because of the limitations as well. It also showed that really hot gas flares can be picked up by VAFP as well, even though it is primarily designed for detecting bigger fire activities like, forest fires and biomass burning.

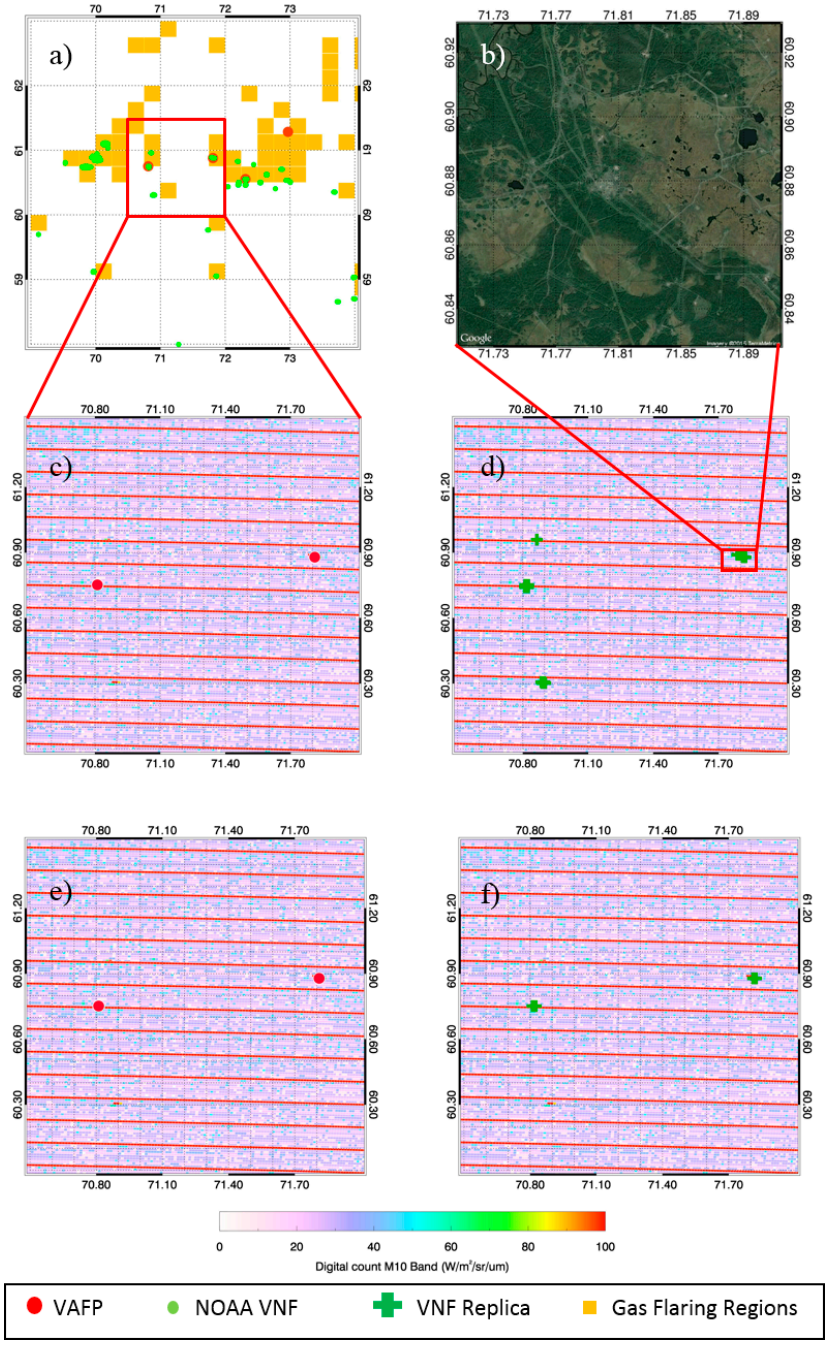

Figure 5. Reconciliation between VAFP and NOAA VNF, 04th July, 2013.

Case 2: August 02nd, 2013; Area (latitude: 60.5°-61.5°, longitude: 70°-71°). 5 counts of fire were detected by the VAFP on the given date during night-time in the small target region, whereas M10 VNF replica detected 20 hotspot (includes all the ones seen by VAFP) counts in the same region (Fig. 6.c, 6d). When the computed VNF Replica M10 threshold (in DC) was increased to 5 times its value, the new replica hotspot count dropped to 15 based on this higher threshold. These new counts still included 4 spots highlighted by VAFP. When the threshold was further increased to 20 times, the replica gave out 10 detections, again having the 4 spots detected by VAFP. 60 times the threshold gave 6 detects, still including 4 locations by VAFP, seen in Fig. 6e and 6f (the two extra

Preprints (www.preprints.org) | NOT PEER-REVIEWED | Posted: 8 May 2017 doi:10.20944/preprints201705.0051.v1

Peer-reviewed version available at Atmosphere 2017, 8, , 95; doi:10.3390/atmos8060095

locations that replica saw had high DN values but were not picked up VIIRS possibly due to cloud cover which is not discarded by VNF). At an even higher threshold (70 times), 3 of the fires picked by AFP originally were still picked up by replica, corroborating the fact VAFP is detecting fires that have very high DN values or are incredibly bright. One of the pixels picked at all thresholds by replica and seen by VIIRS, was clearly showing gas flare flow stations when observed through zoomed in Google image (see Fig. 6b).

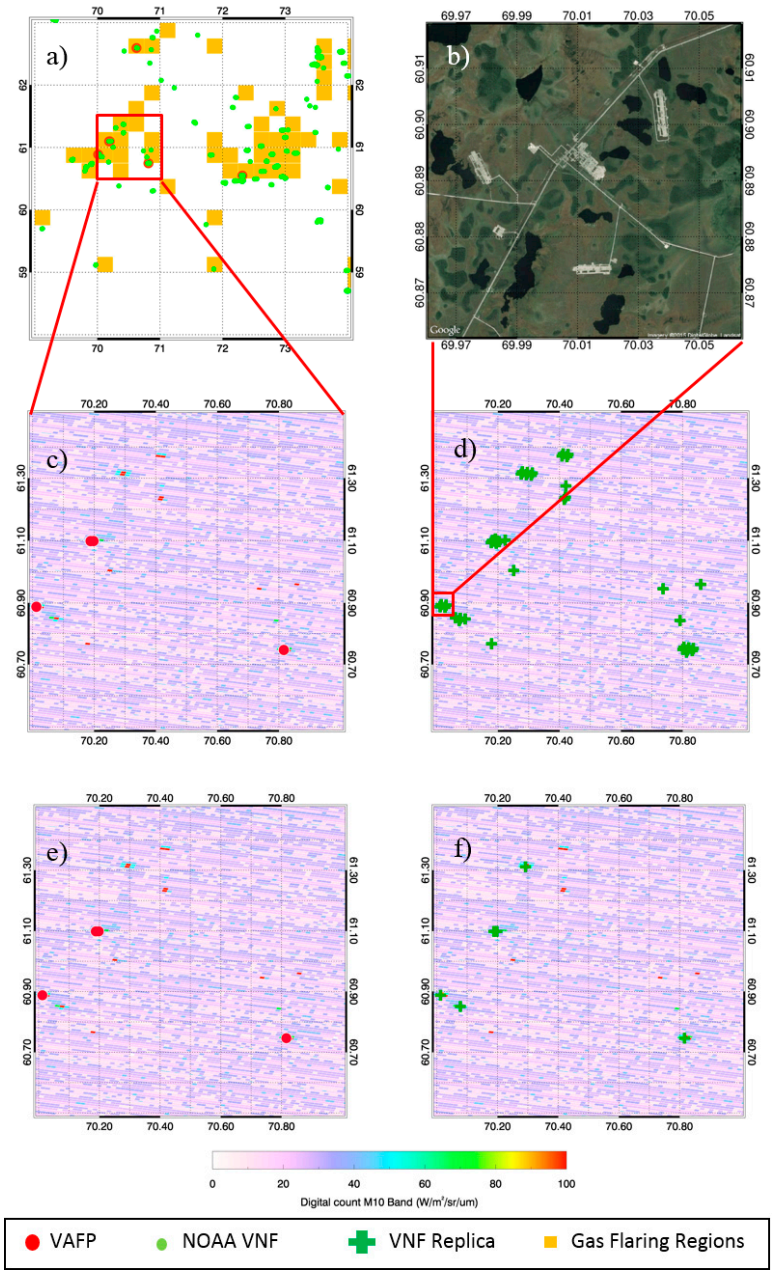

Figure 6. Reconciliation between VAFP and NOAA VNF, 02 August, 2013.

4.2. Reconciliation through theoretical Interpretation

As we observed that VAFP product could also detect some big high temperature flares along with VNF, we looked into the simulated radiances of the primary detection channels of these two products for varying cases of high temperatures and subpixel fire areas. Since the detections by VAFP are mainly based on 4 μm channel and the VNF is based on SWIR bands, principally 1.6 μm, we did a simulation of radiance values in 4um and 1.6 um channels. The objective was to see how

Preprints (www.preprints.org) | NOT PEER-REVIEWED | Posted: 8 May 2017 doi:10.20944/preprints201705.0051.v1

Peer-reviewed version available at Atmosphere 2017, 8, , 95; doi:10.3390/atmos8060095

the TOA (Top-Of-Atmosphere) radiance seen by sensor in these channels varies as the size of the fire or the hotness of the fire changes. The TOA radiance I is represented as:

$$I = (1-A_f)\, I_b(\lambda,T_b) + (A_f)\, I_f(\lambda,T_f)$$

where A_f is the sub-pixel fire fraction, I_b is the spectral radiance contributed by the background pixels (computed by Planck function) and I_f represents the spectral radiance contributed by the flaming part of the pixel at the given wavelength. T_b and T_f represent surface kinetic temperatures of background and fire respectively (Peterson and Wang, 2013).

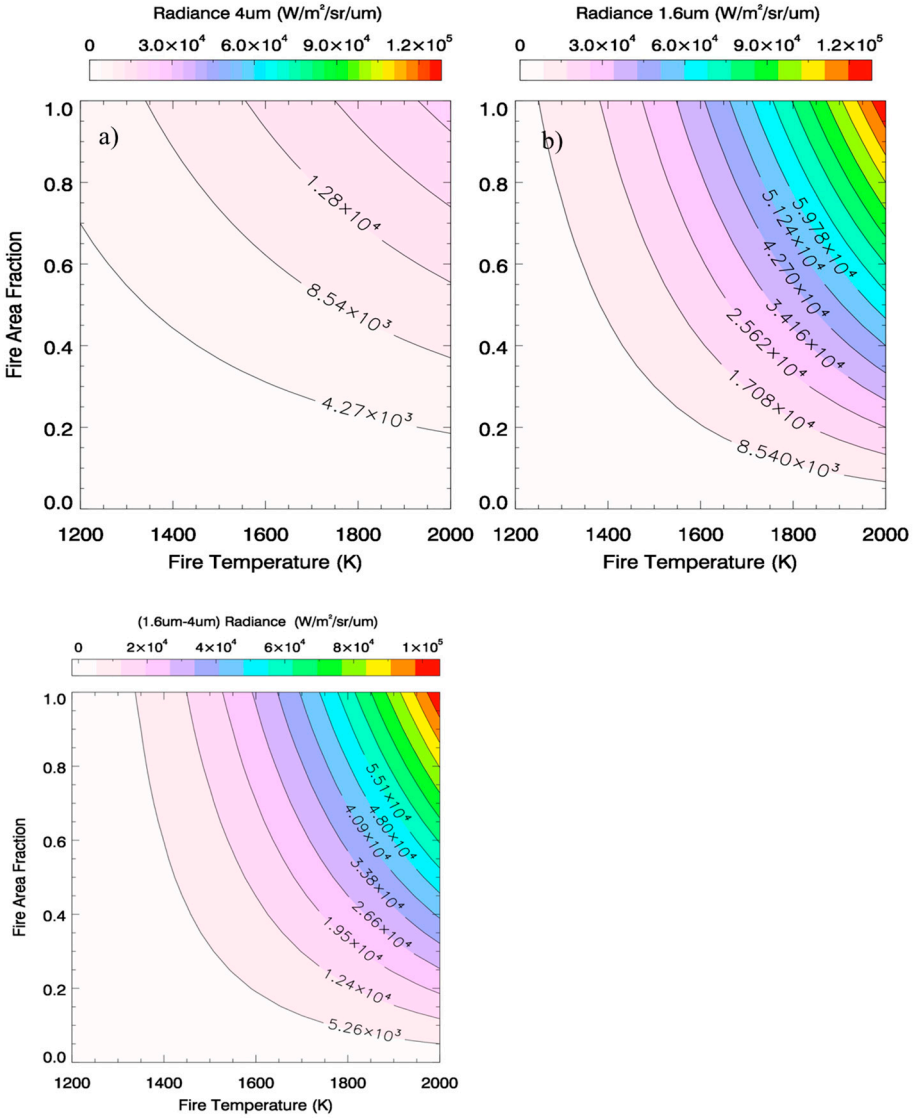

Figure 7. (a) Simulation of 4 μm (top left) and (b) 1.6μm (top right) radiances for varying fire temperature and fire area fraction, as well as (c) their corresponding difference (1.6μm -4 μm) for varying fire temperature and fire area fraction. The brightness temperature for background is considered uniformly at 300 K.

The background temperature was considered as 300 K uniformly for all simulations to represent average surface temperature during summer in West-Siberian, Russia (where the target region is located). Both flaming part of the pixel and background were considered as blackbodies (Giglio and Kendall, 2001) and the atmospheric effects were neglected, so that computed radiances could represent TOA radiance values (Peterson et al., 2013). Figure 7a and 7b respectively show the contour-plot for these simulations for 1.6 μm channel and 4 μm channel. The subpixel fire fractions are varied from 0-100% and the temperatures are simulated for the range 1400-2000 K, to represent hot sources such as flares. Figure 7 shows that the simulated 1.6 μm radiances increase as flare

temperature and subpixel area increases and are much higher than 4 μm radiances, especially for bigger flares at higher temperatures. The result helps in substantiating the sensitivity of SWIR bands to extremely hot sources. It's also notable that 4 μm radiances also increase for high temperature flares with bigger areas, which could possibly explain why some big flares were being detected by these MWIR based VAFP as well. The contour plot of difference of 1.6 and 4 μm radiance is also shown in Figure. 7c. For most part the difference between the radiances is positive and quite high (of the order 10 MW/m²/sr/μm) but for some lower temperature flares with low subpixel area (e.g., whit areas in the figure), the 4 μm radiances were higher than 1.6 μm counterparts, which is expected as the peak radiation tends to shift to higher frequency ranges for sources with cooler temperatures. Hence, for those gas flaring with small areas, only those with very high temperature can be detected by MWIR; however, use of SWIR appears to be efficient in detecting gas flaring for a wide range of temperatures because the background of SWIR is extremely low (as compared to background of MWIR).

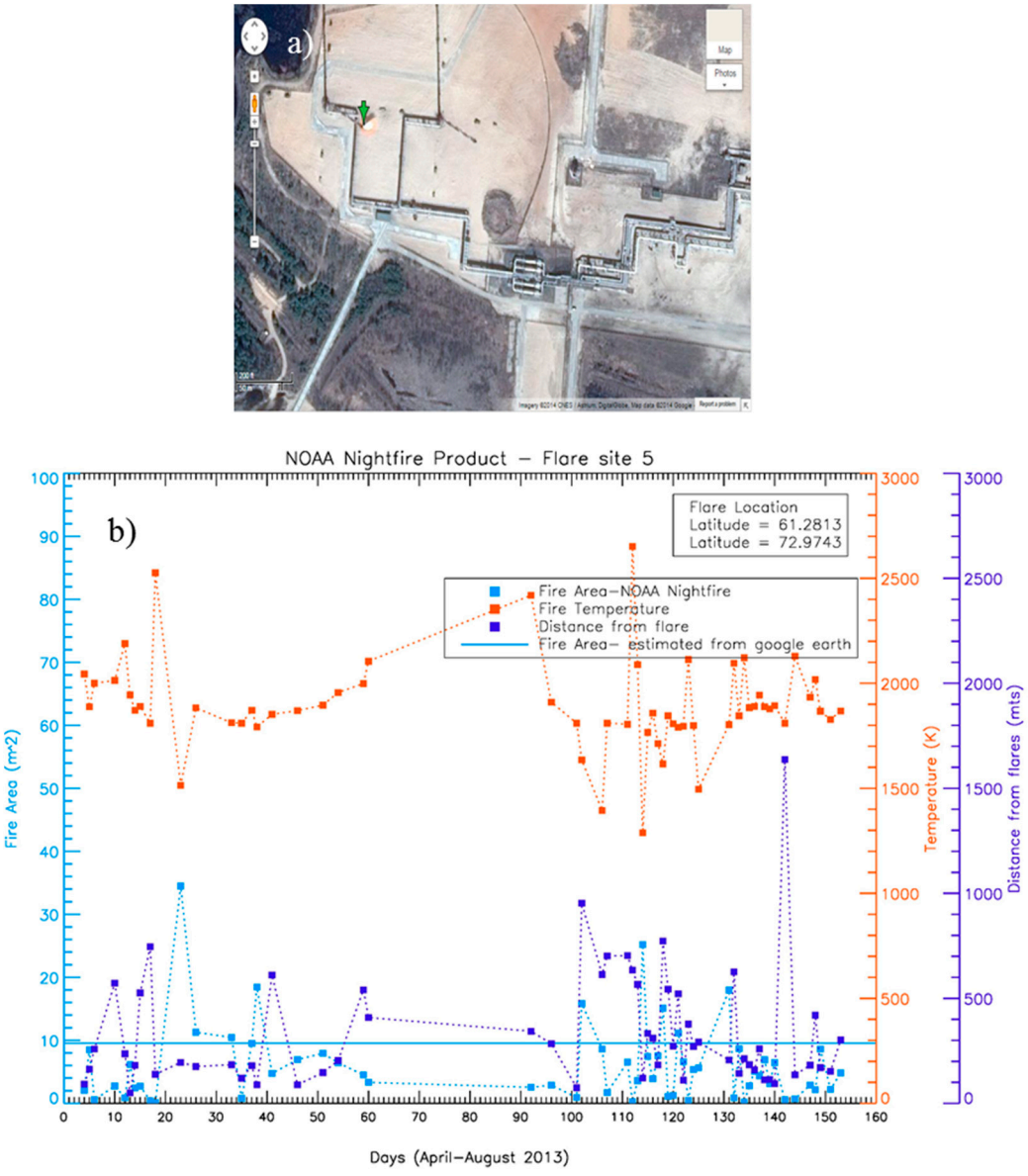

Figure 8. a) A test site in Khanty Mansiysk- Russia (Image courtesy: google maps). 3.7.b) Fire area, temperature and distance of detected pixel from the flare location for this site over 5 months of 2013 retreived from NOAA VNF version 1.0. The red lines represent the fire temperature reported by VNF for hotpixels found in proximity to the flare, whereas the blue and navy blue lines represent the fire area and distance of flare from the center pixel detected, respectively.

Preprints (www.preprints.org) | NOT PEER-REVIEWED | Posted: 8 May 2017 doi:10.20944/preprints201705.0051.v1

Peer-reviewed version available at Atmosphere 2017, 8, , 95; doi:10.3390/atmos8060095

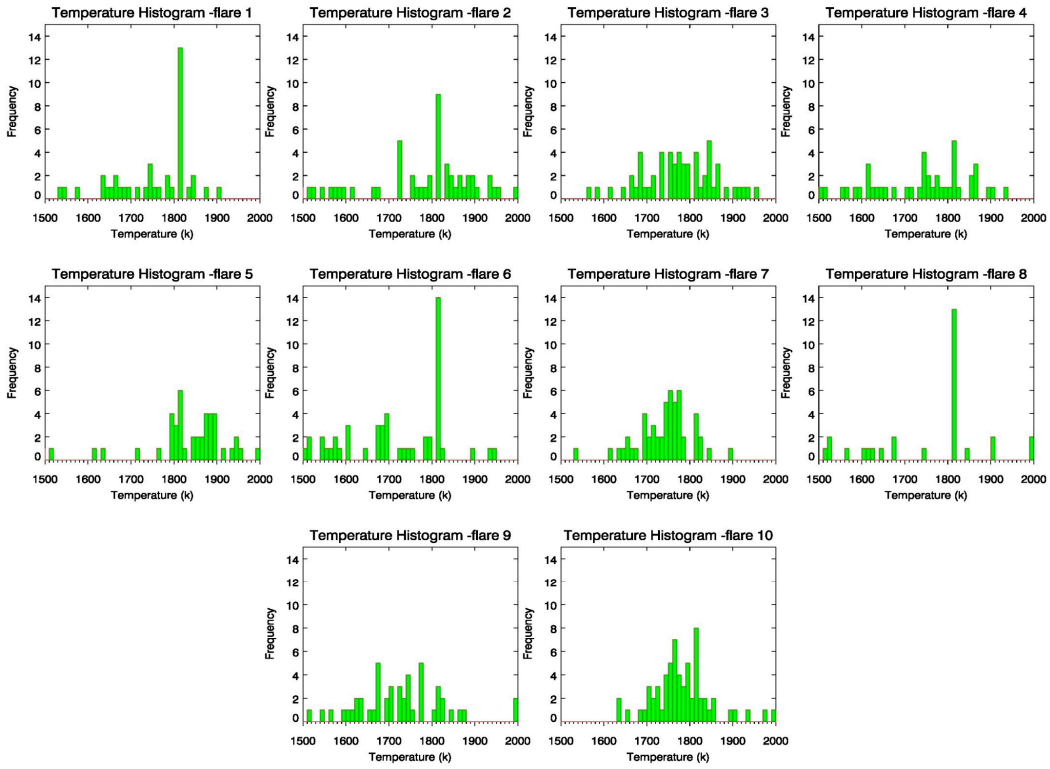

Figure 9. Histogram for fire temperature reported by VNF for 10 chosen flaring sites in the study region over 5 month period (Apr – Aug 2013).

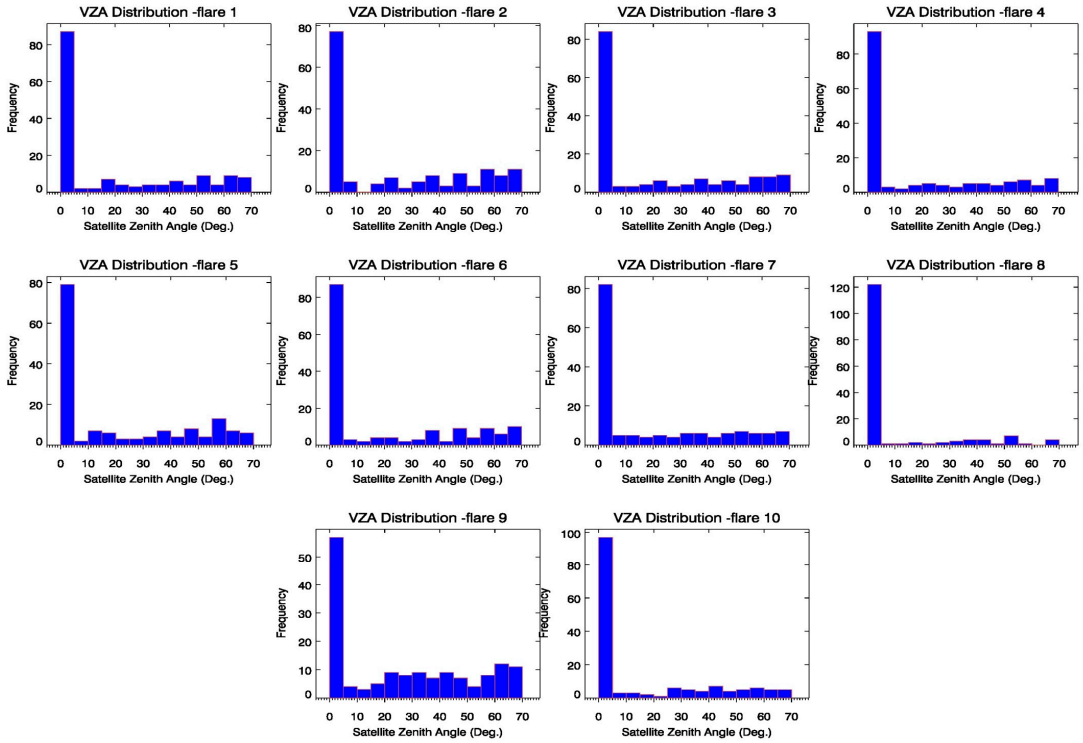

Figure 10. Histogram for view zenith angles for the same period and sites reported by VNF. It is noticeable that most flare detections are happening for viewing angles much closer to Nadir.

5. Evaluation of the Night-fire product for characterizing gas fairing

Since the VNF product is proved to be more effective than other active fire products in detecting gas flares by a considerable margin, we analyzed the collected data (April – August 2013)

Preprints (www.preprints.org) | NOT PEER-REVIEWED | Posted: 8 May 2017 doi:10.20944/preprints201705.0051.v1

Peer-reviewed version available at Atmosphere 2017, 8, , 95; doi:10.3390/atmos8060095

for further evaluation and validation. We chose 10 foreknown gas flaring locations from Google Imagery within the test region boundaries and studied the efficacy of detection of these flares by the product. All the sites were detected many times by the product within the footprint of VIIRS level 2 imagery pixels. The detections where the distance between pixel center and the flare location exceeded 3 kms were discarded and deemed as invalid. Many attributes such as fire area, fire temperature, viewing geometry, radiant heat, radiances in multiple bands, distance from actual flare location etc. associated with valid detections (distance < 3 kms) were stored in a database for further evaluation. The database was created for all 10 different gas flaring sites. Figure 8a shows one such site (Google Image) in Khanty Mansiysk Russia and Figure 8b shows the days of valid detections by the VNF product within the study period along with fire area, fire temperature and distance from the flare.

Table 3 shows the locations of the predetermined flare sites, the no. of times VNF successfully detected them over a period of 5 months, along with mean area, temperature and distance of detection (Euclidean distance between flare site and the center of the nearby pixel showing hotspot). It can be noted here that for almost all the sites, the associated mean temperatures reported by VNF are very high (1600-2000 K). These high mean temperatures corroborate the potential of this product of detecting flares (burning at extremely hot temperatures) with consistency over a long period. The histogram analysis (Fig 9) of temperatures reported for valid detections for all flaring locations under study also exhibits that high temperatures are most frequently associated with these detections.

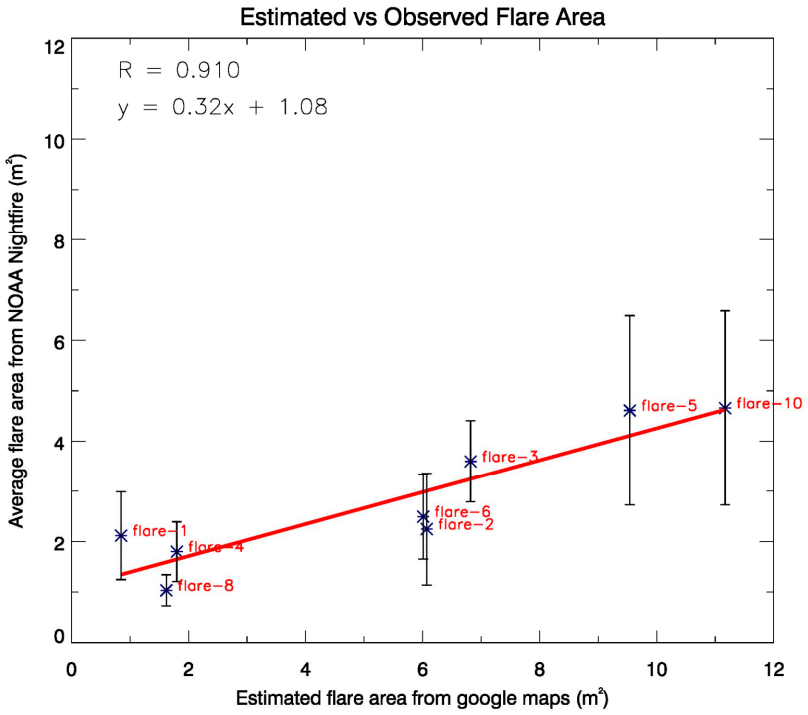

Figure 11. Scatterplot for fire areas reported by NOAA VNF for different flare sites vs the area estimated using google imagery for the respective sites.

Another particular feature is the observation of the view zenith angle, VZA (the angle between local zenith and the line of sight of satellite) associated with valid flare detections (Fig. 10). A histogram of VZA shows that most of the detections are done between (0^0- 5^0), which means that these flares are detected when the satellite overpasses are either directly overhead them or overpasses occur near local nadir for the flares. A plausible reason for this observation is that the small size of flares (the flare area as reported by the VNF product is usually (< 50 m^2) compared to the VIIRS level 2 data pixel size (750 × 750 m) at nadir) makes them hard to detect when seen over a large angle by the satellite instrument. Since flares are mostly found over flare stacks (columns

constructed for safety purposes) and are not spread on ground like biomass burnings or forest fires, the fire area reported is generally confined to the area around the periphery of the flare stacks.

We also verified these fire areas reported by the VNF product for flares under study with the Google Imagery. Triangular areas were drawn around the flare stacks over zoomed in Google Images showing foreknown flare locations and approximate areas around the flares were calculated. It should be noted these are conservative estimates of fire areas for flares and are not representative of exact flame areas as the size of flames depend on various factors like wind speed and fuel burned. Therefore, deducing flare areas from flames isn't very reliable. Verification of areas could not be done for two locations of flares because of the limitation of the available zoomed in google imagery there. Fig. 11 shows a scatter-plot of the comparison between mean of areas reported by VNF and the area estimated by google imagery. In order to remove the bias from the outliers for mean area calculations from the VNF product, the interquartile range ($q_{0.25}$–$q_{0.75}$) of all reported areas was used. The mean and the standard deviation were calculated using the data in this range only. The scatter-plot shows a correlation of 0.910 between the imagery estimated and VNF areas, however VNF is found to underestimate the areas of the flares.

Table 3. Using VNF for long term study of pre-determined flaring locations.

VIIRS VNF Test Sites	Geolocation (degrees)	# of Detections	Mean Fire Area (m^2)	Mean Brightness Temperature (K)	Mean distance of detection (m)
Site 1:	Lat: 60.9704 Lon: 73.8491	*45*	*4.59 ± 7.23*	1773.71 ± *140.868*	402.640 ± *327.470*
Site 2:	Lat: 60.6912 Lon: 72.8564	*62*	*5.37± 11.85*	1789.61 ± *236.843*	768.956 ± *697.082*
Site 3:	Lat: 61.0195 Lon:72.6190	*60*	*3.65 ± 2.08*	1789.20 ± *109.462*	420.553 ± *330.132*
Site 4:	Lat: 61.6430 Lon: 72.1709	*53*	*2.42 ± 2.18*	1773.72 ± *226.354*	370.547 ± *287.388*
Site 5:	Lat: 61.2813 Lon: 72.9743	*60*	*5.95 ± 6.32*	1894.10 ± *222.996*	333.063 ± *275.531*
Site 6:	Lat: 60.7791 Lon:72.7071	*53*	*3.23 ± 3.29*	1710.96 ± *130.777*	358.884 ± *226.843*
Site 7:	Lat:62.4468 Lon:73.5506	*56*	*11.04 ± 7.63*	1728.12 ± *123.712*	418.890 ± *476.166*
Site 8:	Lat: 61.7231 Lon:73.8940	*31*	*1.19 ± 0.77*	1757.84 ± *154.92*	505.728 ± *356.719*
Site 9:	Lat: 62.4922 Lon: 74.4010	*65*	*24.88 ± 16.48*	1788.29 ± *90.1068*	344.189 ± *243.270*
Site 10:	Lat: 60.7386 Lon: 69.9132	*50*	*5.19 ± 4.04*	*1733.50 ± 131.160*	*480.738 ± 315.054*

6. Summary & Discussion

The VNF product was studied for the summer months of 2013 (August-August) in the Khanty Mansiysk Autonomous Okrug – Russia along with other standard fire products. The fire activity

was contrasted and compared for the same period with other fire products such as MOD14 (from MODIS Terra land level 2 data), MYD14 (MODIS Aqua land level2 data) and VIIRS Active Fire Product (VIIRS level 2 data). A broad gas flaring map was made highlighting grids in the target region showing most persistent flaring activity using VNF data. The results revealed that fire counts observed by the VNF product were way higher than the other products both in gas flaring and outside gas flaring zones, with the counts observed by VAFP coming a distant second. The large differences were attributed to the choice of primary detection bands and thresholds involved. The VNF algorithm was replicated using multispectral level 2 VIIRS data to understand its functioning better. Case studies attempting to reconcile the differences between VNF and VAFP showed that the AFP was able to detect flares but only those with very high M10 DN counts (or high radiance).

Upon increasing the thresholds (M10 based) manifold for hot spot detection the VNF replica was able to match detections from AFP. The factor by which thresholds for VNF need to be multiplied to match with AFP is variable. Smaller flares tend to be picked by VNF but are not detected by AFP. In order test the efficacy of the VNF product to detect flares over a longer period of time, the product was tested on pre-specified flaring locations for a period of 5 months. The product did sufficiently well with detecting all the pre-determined flares with frequency touching as high as 40% of the days tested. A database was also created using data associated with the detections by the product. The database included information on viewing geometries, brightness temperatures, fire areas, multispectral radiances etc. Some of the peculiar features of flares shown by the data from database demonstrated that the associated temperatures detected were consistently high > 1600 K almost all the time. Also, a large number of valid detections seemed to have a viewing zenith angle preference (< 5°), which tells the satellites are almost overhead the flares most of the time they are detected, their small size being the most plausible reason. The small size of flares was consistently observed from the VNF as well and on comparison with areas estimated manually from google imagery a good correlation of 0.91 was found between the two. It was also observed that VNF generally underestimates the area of the flares. It should be noted that the area estimated manually is not fully accurate and is a conservative estimate derived by drawing polygon boundaries around flare structure. However, VNF is the among first that shows the capability to characterize gas fairing area from space with good accuracy

Acknowledgments: This project was supported by the NASA's Applied Science Program..

References

1. Anejionu, O. C. D., G. A. Blackburn, and J. D. Whyatt, 2014: Satellite survey of gas flares: development and application of a Landsat-based technique in the Niger Delta. Int.J.Remote Sens., 35, 1900-1925, doi:10.1080/01431161.2013.879351.
2. Casadio, S., O. Arino, and A. Minchella, 2012: Use of ATSR and SAR measurements for the monitoring and characterisation of night-time gas flaring from off-shore platforms: The North Sea test case. Remote Sens.Environ., 123, 175-186, doi:10.1016/j.rse.2012.03.021.
3. Casadio, S., O. Arino, and D. Serpe, 2012: Gas flaring monitoring from space using the ATSR instrument series. Remote Sens.Environ., 116, 239-249, doi:10.1016/j.rse.2010.11.022.
4. Croft, T., 1978: Nighttime Images of Earth from Space. Sci.Am., 239, 86-&.
5. Csiszar, I., W. Schroeder, L. Giglio, E. Ellicott, K. P. Vadrevu, C. O. Justice, and B. Wind, 2014: Active fires from the Suomi NPP Visible Infrared Imaging Radiometer Suite: Product status and first evaluation results. Journal of Geophysical Research-Atmospheres, 119, 803-816, doi:10.1002/2013JD020453.
6. Elvidge, C., M. Imhoff, K. Baugh, V. Hobson, I. Nelson, J. Safran, J. Dietz, and B. Tuttle, 2001: Night-time lights of the world: 1994-1995. Isprs Journal of Photogrammetry and Remote Sensing, 56, 81-99, doi:10.1016/S0924-2716(01)00040-5.
7. Elvidge, C. D., D. Ziskin, K. E. Baugh, B. T. Tuttle, T. Ghosh, D. W. Pack, E. H. Erwin, and M. Zhizhin, 2009: A Fifteen Year Record of Global Natural Gas Flaring Derived from Satellite Data. Energies, 2, 595-622, doi:10.3390/en20300595.

8. Elvidge, C. D., M. Zhizhin, F. Hsu, and K. E. Baugh, 2013: VIIRS VNF: Satellite Pyrometry at Night. Remote Sensing, 5, 4423-4449, doi:10.3390/rs5094423.
9. Gervet, B., "Gas Flaring Emission Contributes to Global Warming," Master's Thesis, Lule University of Technology, Lule, 2007.
10. Giglio, L., J. Descloitres, C. Justice, and Y. Kaufman, 2003: An enhanced contextual fire detection algorithm for MODIS. Remote Sens.Environ., 87, 273-282, doi:10.1016/S0034-4257(03)00184-6.
11. Ichoku, C., Y. Kaufman, 2005: A method to derive smoke emission rates from MODIS fire radiative energy measurements. IEEE Trans.Geosci.Remote Sens., 43, 2636-2649, doi:10.1109/TGRS.2005.857328.
12. Ismail O. and G. Umukoro, "Global Impact of Gas Flaring," Energy and Power Engineering, Vol. 4 No. 4, 2012, pp. 290-302. doi: 10.4236/epe.2012.44039.
13. Justice, C. O., Giglio, L., Korontzi, S., Owens, J., Morisette, J., Roy, D., Descloitres, J., Alleaume, S., Petitcolin, F. and Kaufman, Y. J. 2002. The MODIS fire products. Remote Sensing of Environment 83:244-262. doi:10.1016/S0034-4257(02)00076-7
14. Knizhnikov, A., Poussenkova, N., 2009: Russian Associated Gas Utilization: Problems and Prospects, Annual Report within the Framework of the Project, Environment and Energy
15. Mebust, A. K., A. R. Russell, R. C. Hudman, L. C. Valin, and R. C. Cohen, 2011: Characterization of wildfire NOx emissions using MODIS fire radiative power and OMI tropospheric NO2 columns. Atmospheric Chemistry and Physics, 11, 5839-5851, doi:10.5194/acp-11-5839-2011.
16. Muirhead, K., A. Cracknell, 1984: Identification of Gas Flares in the North-Sea using Satellite Data., *Int.J.Remote Sens.*, 5, 199-212.
17. Nwanya, S. C., 2011: Climate change and energy implications of gas flaring for Nigeria. International Journal of Low Carbon Technologies, 6, 193-199.
18. Peterson, D. and J. Wang, A Sub-pixel-based calculate of fire radiative power from MODIS observations: 2. Sensitivity analysis and potential fire weather application, *Remote Sensing Environment*, 129, 231-249, 2013.
19. Polivka, T., E. Hyer, J. Wang, and D. Peterson, First global analysis of saturation artifacts in the VIIRS infrared channels and the effects of sample aggregation, *IEEE Geoscience and Remote Sensing Letters*, 1262-1266, 2015.
20. Ross, A. N., M. J. Wooster, H. Boesch, and R. Parker, 2013: First satellite measurements of carbon dioxide and methane emission ratios in wildfire plumes. Geophys.Res.Lett., 40, 4098-4102, doi:10.1002/grl.50733.
21. Weaver, J., D. Lindsey, D. Bikos, C. Schmidt, and E. Prins, 2004: Fire detection using GOES rapid scan imagery. Weather and Forecasting, 19, 496-510, doi:10.1175/1520-0434(2004)019<0496:FDUGRS>2.0.CO;2.
22. Wooster, M., G. Roberts, G. Perry, and Y. Kaufman, 2005: Retrieval of biomass combustion rates and totals from fire radiative power observations: FRP derivation and calibration relationships between biomass consumption and fire radiative energy release. J.Geophys.Res.-Atmos., 110, D24311, doi:10.1029/2005JD006318